Arabian Journal of Chemistry (2023) **16**, 104808

King Saud University

Arabian Journal of Chemistry

www.ksu.edu.sa
www.sciencedirect.com

ORIGINAL ARTICLE

Mxene $Ti_3C_2T_x$ derived lamellar $Ti_3C_2T_x$-TiO_2-CuO heterojunction: Significantly improved ammonia sensor performance

Ming Hou [a], Guoxin Jiang [a], Shenghui Guo [a], Jiyun Gao [a], Zhigang Shen [d], Zhihang Wang [f], Xiaolei Ye [b,*], Li Yang [a,c,*], Qian Du [a], Jianhong Yi [e], Hongbo Zeng [c], Pascal Briois [b]

[a] *State Key Laboratory of Complex Nonferrous Metal Resources Clean Utilization; Faculty of Metallurgical and Energy Engineering, Kunming University of Science and Technology, Kunming 650093, China*
[b] *FEMTO-ST Institute (UMR CNRS 6174), UBFC/UTBM. Site de Montbéliard, F-90010 Belfort, France*
[c] *Department of Chemical and Materials Engineering, University of Alberta, Edmonton T6G 2V4, Canada*
[d] *SINOPEC Shanghai Research Institute of Petrochemical Technology, Shanghai 201208, China*
[e] *Faculty of Materials Science and Engineering, Kunming University of Science and Technology, Kunming 650093, China*
[f] *Sinochem International Corporation, Beijing 100045, China*

Received 25 November 2022; accepted 11 March 2023
Available online 18 March 2023

KEYWORDS

MXene $Ti_3C_2T_x$;
UV irradiation;
MXene-TiO_2-CuO heterojunction;
Gas sensor;
NH_3

Abstract Ammonia (NH_3), as main industrial gas emissions, are extremely harmful to the human beings. So the detection of NH_3 concentrations in special environments at room temperature (25 °C) is essential. Herein, the composite MXene $Ti_3C_2T_x$-TiO_2-CuO was successfully prepared by one-step *in-situ* oxidation method using $Cu(NO_3)_2{\cdot}6H_2O$ as a precursor. The morphology of $Ti_3C_2T_x$-TiO_2-CuO shows layered accordion-like structure. $Ti_3C_2T_x$-TiO_2-CuO sensor exhibits improved NH_3 gas sensing response of 56.9 toward 100 ppm NH_3 at room temperature under ultraviolet (UV) light exposure, which is 89.8 % higher than that of pristine $Ti_3C_2T_x$ material. The improved gas sensing performance is attributed to the irradiation of UV light, the retention of $Ti_3C_2T_x$ layered structure and the construction of TiO_2-CuO heterojunction. Further, the possible gas sensing mechanism of the material was proposed and discussed.

* Corresponding authors.
E-mail addresses: xiaolei.ye@utbm.fr (X. Ye), yanglikmust@163.com (L. Yang).

https://doi.org/10.1016/j.arabjc.2023.104808
1878-5352 © 2023 The Author(s). Published by Elsevier B.V. on behalf of King Saud University.

1. Introduction

In the past decades, atmospheric environmental pollution has been a major problem plaguing most countries in the world (Chan and Yao, 2008). NH_3, as one of the atmospheric pollutants, is the main cause of acid rain. Long-term inhalation of NH_3 will cause pulmonary edema, respiratory distress syndrome and other diseases, which will cause serious harm to the human body (Shkir et al., 2022; Qin et al., 2022; Khudher and Abd, 2021; Alothman and Wabaidur, 2019; Late et al., 2014; Wu et al., 2018). Therefore, the development and preparation of gas sensing materials with excellent NH_3 gas sensing properties have always been an important topic of concern. Addressing the above issues, researchers have carried out extensive and in-depth research on the exploration of gas sensing materials and the preparation of gas sensors. Among many gas sensing materials, metal oxide semiconductor (MOS) has received extensive researches and attentions, such as SnO_2, TiO_2, ZnO, CuO, WO_3 and so on (Lei et al., 2020; Meng et al., 2015; Xu et al., 2022; Aliha et al., 2013; Kou et al., 2016; Li et al., 2022; Zhou et al., 2021; Wang et al., 2021). Shahabuddin et al prepared NH_3 gas sensor based on SnO_2 films modified with metallic clusters (MCS). And they investigated the effect of ion species on the gas sensing properties of SnO_2. The results show that the integration of Pt is beneficial for enhancing the gas sensing properties of SnO_2, it shows a high response value of 25.7 toward 450 ppm NH_3 at 230 °C (Shahabuddin et al., 2014). Srinivasulu et al fabricated a 2D ZnO gas sensor, which displays ultra-fast gas sensing response to NH_3. The sensor exhibits a maximum response of 80% toward NH_3 at 250 °C (Kanaparthi and Singh, 2020). Obviously, MOS-based gas sensors have shown excellent gas sensitivity. However, they usually require high operating temperatures to ensure electrons transfer from Valence Band (VB) to Conduction Band (CB). The high working temperature makes the gas sensor unstable, and confines the utilization in complex atmosphere environment and flexible devices. Thus, it is important to search a low/room-temperature gas sensing material to replace MOS or devise a novel method to reduce operating temperature.

MXene as a promising two-dimensional (2D) material introduces the special characteristics and advantages, such as high specific surface area, abundant functional groups. Typically, $Ti_3C_2T_x$ (T_x represents, -F, –OH and -O) is the most widely studied MXene because of its superior electrical conductivity, organ-like structure and mature fabrication process (Akhtar et al., 2021; Xu et al., 2017; Deng et al., 2022; Yuan et al., 2018; Chen et al., 2019; Xie et al., 2018), which make it the preferred material for gas sensing field. Although several works have been done to investigate the gas sensing properties of MXene and they have shown good selectivity for NH_3 and VOCs (Sun et al., 2020; Kim et al., 2018; Gasso et al., 2022; Li et al., 2021; Zhao et al., 2021; Zhao et al., 2020; Zhang et al., 2022). There are still large challenges for improvement in the gas sensitivity of the material. On the basis of the working mechanism of resistive gas sensor, the gas sensitivity can be enhanced by constructing the heterostructure to build energy level interleaving effect, which can effectively promote the separation of free carriers, so that more free charges can take part in the gas–solid reaction and improve the gas sensitivity (Miller et al., 2014; Hang et al., 2017).

As is well known, titanium dioxide (TiO_2) has been widely studied in photocatalytic and gas sensing fields because of high stability, high electrochemical performance, and excellent catalytic performance (Lai et al., 2010; Chen et al., 2012; Wang et al., 2011; Zhang et al., 2014). At the same time, in order to improve the gas sensing properties of TiO_2 and broaden its application in gas sensing materials, a lot of works have been done to combine TiO_2 with CuO to form p-n heterojunction. The construction of p-n heterojunction is conducive to electron-hole separation, so that more carriers participate in interfacial chemical reactions. Alev et al. (Alev and Sennik, 2018) prepared CuO thin film-TiO_2 nanotube heterojunction composites by thermal oxidation evaporation method. The results show that the heterojunction materials have better gas sensing properties and lower working temperature than pure CuO and TiO_2. At the same time, the formation of heterojunction materials can enhance gas sensing properties toward H_2 and reduce the gas sensing properties of VOCs and NO_2, so as to improve the gas sensing selectivity of materials. In summary, the construction of TiO_2-CuO heterojunction can effectively enhance the gas sensitivity of materials. What's more, CuO is a narrow band gap semiconductor, and the combination of CuO and TiO2 can improve the photocatalytic performance. With the help of the photosensitive properties of CuO-TiO2, the photothermal combined excitation can be realized by means of light excitation, which can improve the carrier migration speed and improve its gas sensitivity. It is worth noting that MXene $Ti_3C_2T_x$ may be in-situ transformed partly to an n-type TiO_2 semiconductor via oxidation to form MXene-TiO_2 heterojunction and it can still retain the original organ-like layered structure. This special structure can provide high-speed channels for electron transmission, so as to improve the gas sensitivity of the material (Wang et al., 2009). Thus, one-step in-situ oxidation could be applied to fabricate $Ti_3C_2T_x$-TiO_2-CuO heterojunction to enhance the gas sensitivity of MXene. What's more, changing the free carrier excitation source from traditional thermal excitation to light excitation is also an effect method to reduce operating temperature. The sensing materials could be irradiated by sufficient light energy, which make the valence band (VB) electron transition to obtain free electrons to achieve gas sensing response (Karaduman et al., 2014; Cui et al., 2016). In addition, light irradiation is conducive to boosting the response and improving the response/recovery features. Therefore, combining heterojunction construction with photo excitation will be a new breakthrough in the field of MXene gas sensing materials.

Herein, we demonstrate the achievement of room temperature gas sensing materials is in accordance with the formation of MXene Ti_3C_2-T_x-TiO_2-CuO heterojunction and the illumination of UV light. TiO_2 were formed in-situ on the in-layer and surface of MXene to construct MXene-TiO_2 junction, which was achieved through one-step in-situ oxidation. The existence of $Ti_3C_2T_x$-TiO_2-CuO junctions was confirmed using field emission scanning electron microscopy (FESEM). The optimized MXene $Ti_3C_2T_x$-TiO_2-CuO material demonstrated gas sensitivity superior to that of pristine $Ti_3C_2T_x$, TiO_2-CuO and Ti_3C_2-T_x-TiO_2 toward NH_3. The existence of UV light is beneficial to the gas sensitivity of $Ti_3C_2T_x$-TiO_2-CuO materials.

2. Materials and methods

2.1. Methods of sample preparation

Synthesis of $Ti_3C_2T_x$ MXene: 1 g lithium fluoride (LiF ≥ 99 %) powder was dissolved in 10 mL 9 mol/L hydrochloric acid (HCl) and stirred at room temperature for 30 min. 1 g of Ti_3AlC_2 MAX powder was slowly added into the above solution in the ice bath, and then the solution was sealed and transferred to oil bath at 35 °C for continuous stirring for 24 h. The obtained precipitate was repeatedly centrifuged and washed with deionized (DI) water at 3500 r/min for 5 min each time until the pH value of the solution was neutral. At last, the as-prepared samples were put into an oven for drying at 80 °C.

Synthesis of $Ti_3C_2T_x$-TiO_2-CuO: Different mass (0.01 g, 0.05 g and 0.1 g) copper nitrate ($Cu(NO_3)_2{\cdot}6H_2O$) was dispersed uniformly in 1 mL DI water, respectively. 1 g $Ti_3C_2T_x$ powder was put into the above dark blue solution, and the black uniform $Ti_3C_2T_x$ /$Cu(NO_3)_2{\cdot}6H_2O$ solution was obtained by magnetic stirring for 15 min at room temperature. Stand in dark at room temperature for 24 h to fully volatilize the liquid phase and obtain black precipitate. The obtained samples were then placed in an oven and dried at 70 °C for 8 h. Then put into a tube furnace and sintered at 500 °C for

30 min under the protection of argon (Ar, 99.99%) to obtain $Ti_3C_2T_x$-TiO_2-CuO composites with different CuO contents.

$Ti_3C_2T_x$-TiO_2 and TiO_2-CuO composites were also prepared to investigate the effects of $Ti_3C_2T_x$ and CuO additions on the material performances. The preparation details are as follows: 1 g of $Ti_3C_2T_x$ powder was put into the Al_2O_3 ceramic crucible, and sintered at 200 °C for 60 min in air atmosphere to obtain black powdered $Ti_3C_2T_x$-TiO_2 composites. 0.1 g Cu $(NO_3)_2{\cdot}6H_2O$ and 1 g $Ti_3C_2T_x$ powder were dispersed uniformly in 1 mL DI water by using magnetic stirring. Then stand in dark at room temperature for 24 h to fully volatilize the liquid phase and obtain black precipitate. After drying at 70 °C for 8 h in an oven, the obtained samples were put into a tuber furnace and sintered at 500 °C in air atmosphere for 30 min to obtain TiO_2-CuO composite (Fig. 1). To better distinguish samples, $Ti_3C_2T_x$-TiO_2-CuO composites with 0.01 g, 0.05 g and 0.1 g $Cu(NO_3)_2{\cdot}6H_2O$ were labeled as TTC-1, TTC-2 and TTC-3, respectively. $Ti_3C_2T_x$-TiO_2 and TiO_2-CuO complex were labeled as TT and TC, respectively.

2.2. Samples characterization

The morphologies of samples were observed by a field emission scanning electron microscope (FESEM, JSM-5610L). The distribution of Ti and Cu and the location of TiO_2 and CuO were confirmed by using Energy Disperse Spectroscopy (EDS). N_2 adsorption/desorption (Autosorb-1-C) method was used to measure specific surface area at 77.4 K. X-ray diffraction (XRD, Rigaku D/max-2500) was applied to study the crystal phase in the 2θ range from 10° to 90°.

2.3. Measurement of gas sensing performance

In order to get the dynamic resistance of sensors, the prepared samples were printed on the chips composed with heating electrode and measuring electrode by using screen printing process. It is worth noting that the detail information about the chips is described in supply materials (Hou et al., 2021; Hou et al., 2021). Then the chips with different samples were put into an oven to evaporate and remove moisture at 70 °C for 40 min and annealed at 400 °C for 2 h under Ar atmosphere.

The prepared chips were mounted in a four-channel gas sensitivity detection equipment to measure gas sensing sensitivities. Target gases were diluted with air, and desired gas concentrations were obtained by controlling the flow rates in a home-made gas delivery system. The operating temperature were maintained range from 25 to 300 °C to investigate the gas sensitivity of samples at different temperatures. The resistance signal of samples was collected by data collection module (Agilent 34970A). The gas responses of samples were calculated based on the change of resistance, and the detail formula is shown as following:

$$S = \frac{\Delta R}{R_a} \times 100\% \tag{1}$$

where ΔR is resistance difference under air and target gas. R_a equals to the resistance under air.

3. Results and discussion

In order to study the information of the prepared samples, XRD was used to analysis phase structure of all samples and the results are shown in Fig. 2. Fig. 2**(a)** shows the XRD patterns of Ti_3AlC_2 before and after hydrofluoric acid etching. It can be seen that there exist Ti_3AlC_2 peak in the spectrum before etching, and the characteristic peaks of $Ti_3C_2T_x$ appeared at 18.2°, 27.5°, 35.9°, 41.7° and 60.4° in the spectrum after etching. At the same time, there was no residual peak of Ti_3AlC_2 in the spectrum, indicating that the Al layer in Ti_3AlC_2 was etched completely by hydrofluoric acid and the pristine $Ti_3C_2T_x$ material was successfully prepared. Fig. 2**(b)** displays X-ray diffraction (XRD) patterns of each sample fabricated with one-step in-situ oxidation method. $Ti_3C_2T_x$, TiO_2 (25.34°, 37.9°, 48.17°, 54.02° and 55.16°) can be observed in TTC-1, TTC-2 and TTC-3 spectra, indicating that TiO_2 has been loaded on $Ti_3C_2T_x$, while $Ti_3C_2T_x$ phase still exists in the three samples, demonstrating that $Ti_3C_2T_x$ is not completely oxidized. CuO phase was not found in the diffraction pattern of all samples, which is related to the low content of CuO. XRD cannot identify the phase when the content is less than 5% (Amparo et al., 2008; Ciżmana, 2020). There is no diffraction peak of MXene, which demonstrates MXene has been transferred to TiO_2 completely. In the diffraction pattern of TT sample, $Ti_3C_2T_x$ and TiO_2 diffraction peaks can also be observed, proving that $Ti_3C_2T_x$ and TiO_2 were successfully combined.

In order to investigate $Ti_3C_2T_x$ and TiO_2-CuO compound state, FESEM was applied to check the microstructure of all samples. The results are shown in Fig. 3. It can be seen from Fig. 3**(a)-3(b), 2D** $Ti_3C_2T_x$ prepared by etching Ti_3AlC_2 with fluoride salt (LiF, HCl) system has typical accordion-like morphology, which is composed of a large number of layers, and

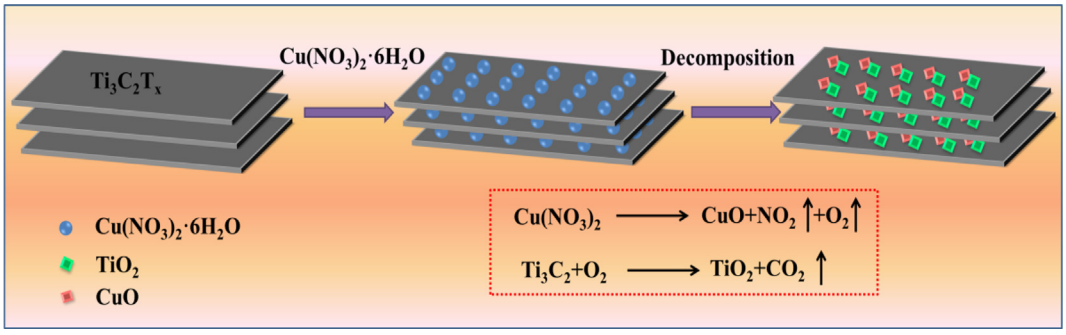

Fig. 1 The schematic diagram of the manufacture of $Ti_3C_2T_x$-TiO_2-CuO.

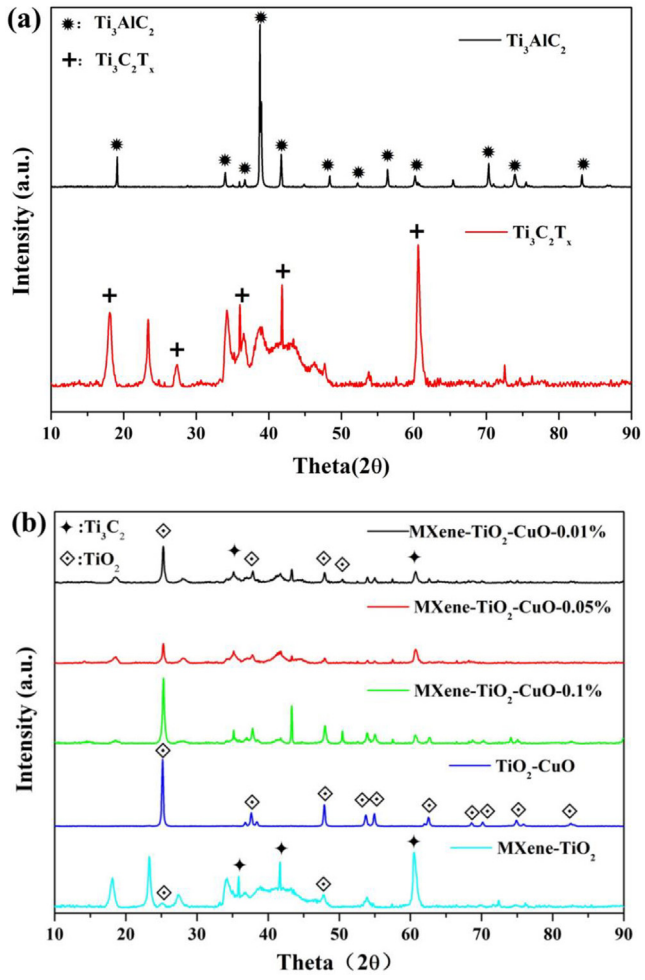

Fig. 2 XRD spectra of Ti_3AlC_2, $Ti_3C_2T_x$, TTC-1、TTC-2, TTC-3, TT and TC composites.

the layers are arranged in neat rows in the absence of impurities. Obvious white particles can also be observed on the surface of $Ti_3C_2T_x$ composited with different contents of CuO (Fig. 3**(c-e)**). In order to trace the distribution of TiO_2 and CuO, EDS was used to characterize and analyze the distribution of different elements. Taking TTC-1 for example, TTC-1 was characterized and analyzed by EDS, the results are shown in Fig. 4**(a–d)**. C, O, F, Al, Ti and Cu elements appear at points 1 and 2. Cu account for a large proportion in point 1, and the Ti mainly concentrates at point 2 and 3, indicating that the scab attached to the surface of $Ti_3C_2T_x$ is TiO_2, and the white particle is CuO, which proves that the TiO_2-CuO heterojunction is successfully combined with $Ti_3C_2T_x$. The adhesion of TiO_2-CuO heterojunction on the surface of $Ti_3C_2T_x$ is conducive to increasing the specific surface area of the material and improving the gas adsorption surface active sites, thereby improving the gas sensitivity of the material.

Fig. 4**(e)** exhibits the microstructure of the TT sample. After sintering at 200 °C, fine particles appear on the surface of $Ti_3C_2T_x$, and $Ti_3C_2T_x$ still maintains a layered structure, indicating that low temperature sintering cannot cause damage to the structure of $Ti_3C_2T_x$ material. Combined with the analysis results of XRD in Fig. 3, the $Ti_3C_2T_x$-TiO_2 composite was successfully prepared. The TiO_2-CuO sample prepared by high temperature (500° C) sintering in air atmosphere shows a rough stacked morphology (Fig. 3**(g-h)**), and the original smooth and angular morphology disappeared, combined the results of XRD in the diffraction peak of TC, indicating that $Ti_3C_2T_x$ was completely oxidized to TiO_2. EDS surface scanning characterization was carried out to verify the existence of CuO and the results are shown in Fig. 4**(d-e)**. The scanned area contains C, O, Ti, Al and Cu elements, indicating the existence of CuO phase, but the content of Cu element is less than 5%, which is the reason why CuO phase cannot appear in the XRD TC sample pattern.

Table 1 shows the specific surface area of raw $Ti_3C_2T_x$ and $Ti_3C_2T_x$ based composites. It can be seen from the result that TTC composites has a higher specific surface area. And the value of TTC-1 sample is 80.9 m^2 /g, which is 70.6 % higher than that of raw $Ti_3C_2T_x$ sample. There is no obvious or even decreasing trend in specific surface area of TT sample, because $Ti_3C_2T_x$ was in-situ oxidized into TiO_2, which destroyed the original layered structure and reduced the specific surface area of the sample.

In order to study the effect of TiO_2-CuO and CuO addition on the gas sensitivity of $Ti_3C_2T_x$ materials, the gas sensing response values of different samples were tested. Firstly, the gas sensitivity values of all samples to 100 ppm NH_3 under UV irradiation at different working temperatures were studied. The results are shown in Fig. 5**(a)**. The gas sensitivity of different samples shows high dependence on working temperature. After the composite of $Ti_3C_2T_x$ and $Cu(NO_3)_2$ with different contents (0.01 %, 0.05 % and 0.1 %), and the gas sensing properties of TTC-1, TTC-2 and TTC-3 are improved at all temperatures. Among them, TTC-1 shows the highest gas sensing response in the measurement at 100 °C when the temperature limited within 100 °C. This is because $Ti_3C_2T_x$ was compounded with 0.01 % $Cu(NO_3)_2$, and the generated TiO_2-CuO was attached to the surface of $Ti_3C_2T_x$ material, which increased the specific surface area of the material and provided more active sites for gas adsorption, thereby significantly improving the gas sensing properties. With increasing the content of $Cu(NO_3)_2$, the decomposed O_2 increases, and the TiO_2-CuO particles grow up. The large particles could partially block the $Ti_3C_2T_x$ layer, which is not conducive to electronic transmission, so that the gas sensitivity of the material is not significantly improved or even unfavorable. The gas response value of TTC-1 is 56.9% toward 100 ppm NH_3 at room temperature, which is 89.8 % higher than that of raw $Ti_3C_2T_x$ sample. At the same time, the optimal operating temperature of TTC-1 sample is 100 °C, and gas sensitivity response value is 91.1 %, indicating the addition of TiO_2-CuO is beneficial for the improvement of gas performance of $Ti_3C_2T_x$. For TC sample, the gas sensing performance is lower than that of raw $Ti_3C_2T_x$ at 25–100 °C. The target gas does not have enough energy to react with the adsorbed oxygen on the material surface at low temperature, and the carrier transition ability is insufficient, which makes the response value low. As the temperature increases, the gas response value of the TC sample shows higher than that of pristine $Ti_3C_2T_x$ sample at 150–300 °C. At the moment, the target gas molecules become sufficiently active, and the carriers obtain sufficient energy to transition to the surface of the material for adsorption chemical reaction, resulting in a significant increase in the response value. The optimal gas sensing temperature of TC sample is 200 °C. It is worth mentioning that STTC-1

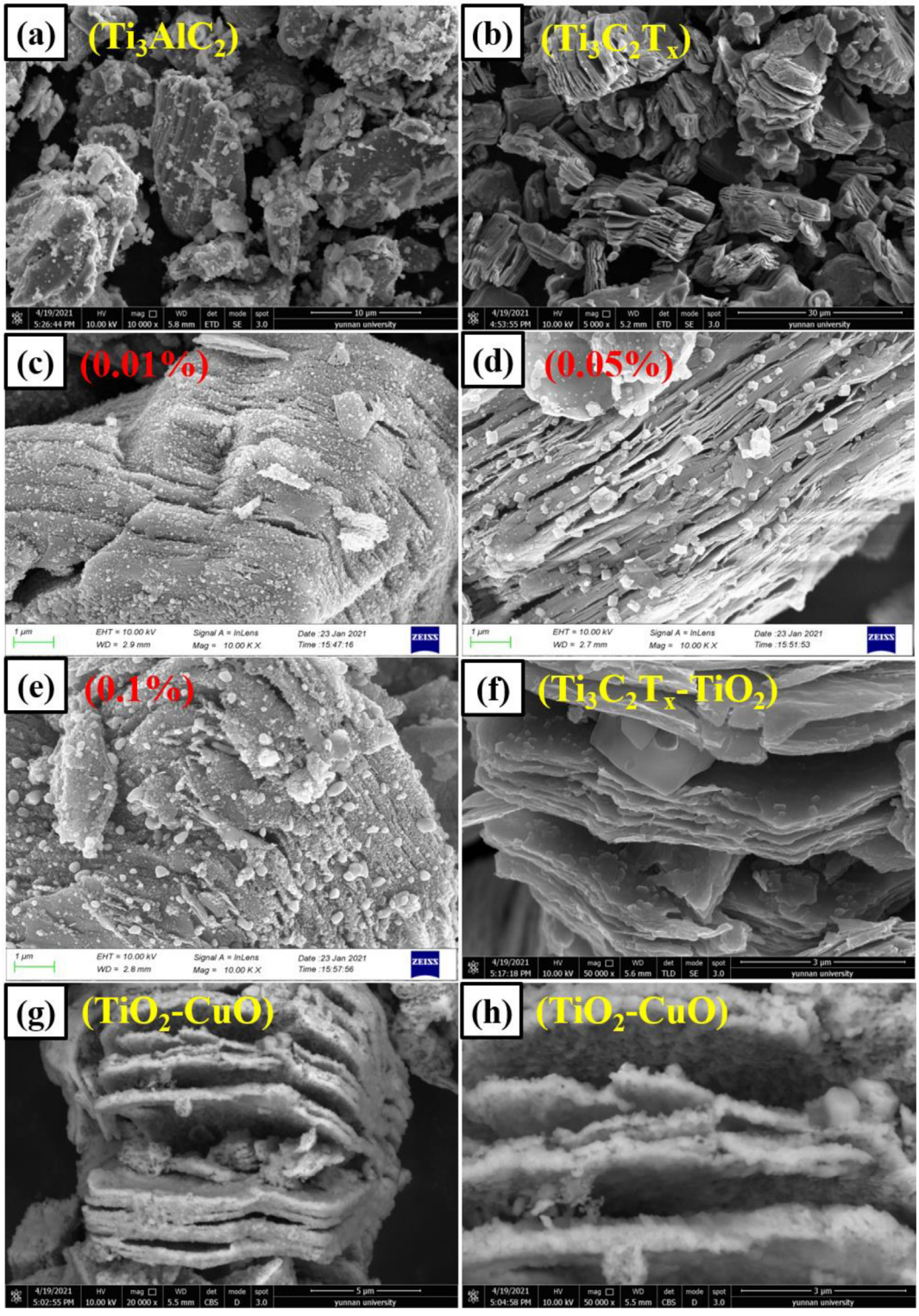

Fig. 3 FESEM images of Ti_3AlC_2、$Ti_3C_2T_x$、TTC-1、TTC-2、TTC-3、TT and TC.

(100 °C) > STC (200 °C). This is because $Ti_3C_2T_x$ material in TTC-1 is not completely oxidized and still retains the layered structure, it can provide high-speed migration channels for carriers in the process of gas sensing reaction, effectively avoids the previous carrier needs to cross the grain boundary barrier to complete the transmission, improving the gas sensitivity of the material. In order to investigate the influence of CuO addition on the gas sensitivity of materials, the gas sensing properties of TT samples were also tested. The results exhibits that the existence of CuO can increase the gas sensitivity of samples, which is because CuO could form TiO_2-CuO heterojunction with TiO_2. The construction of heterojunction is

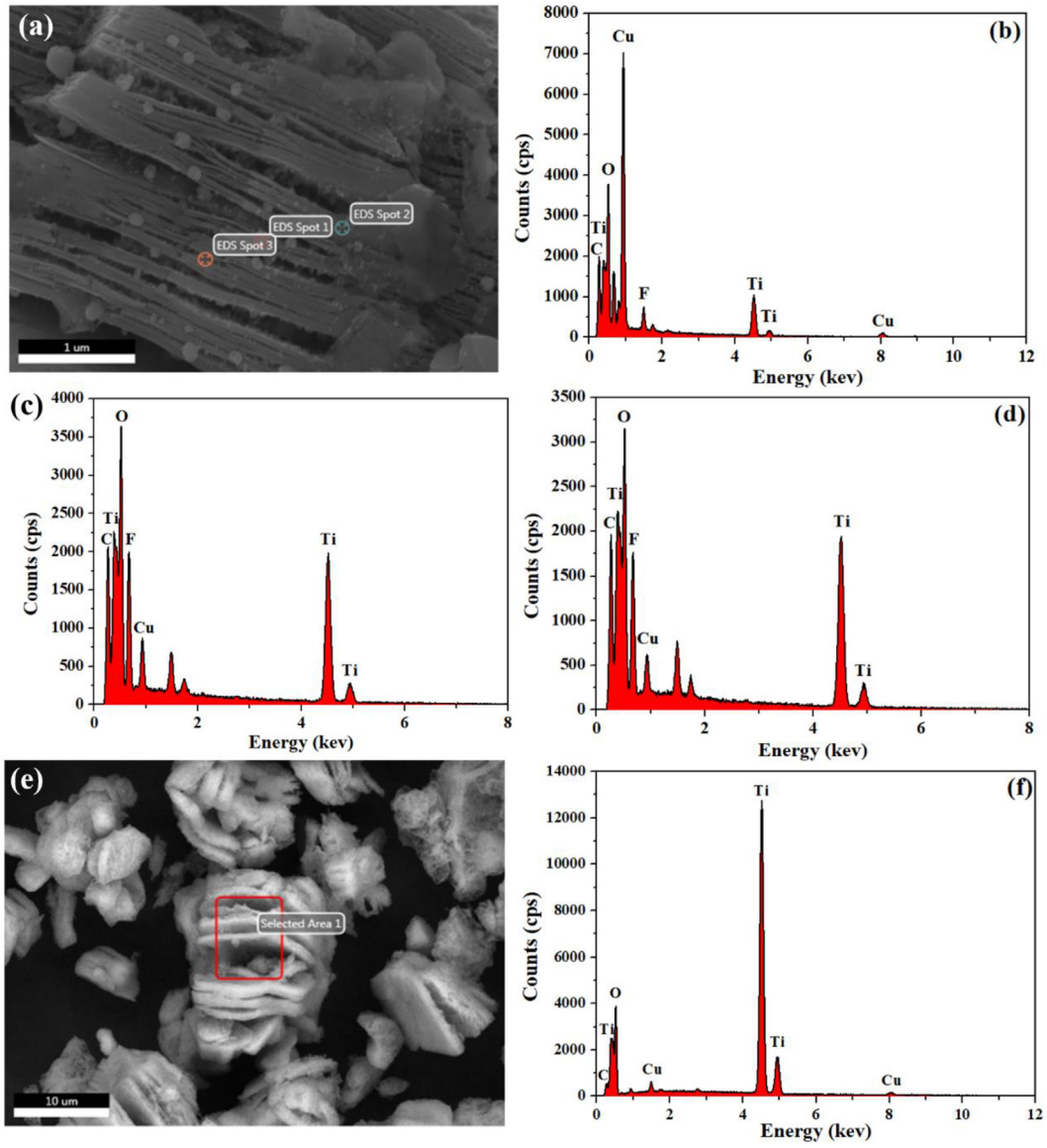

Fig. 4 EDS spectra of TTC-1 (a, b, c, d) and EDS mapping of the marked domain of TC (e, f).

Table 1 Specific surface area of $Ti_3C_2T_x$ and different composite materials.

Sample	$Ti_3C_2T_x$	TTC-1	TTC-2	TTC-3	TT	TC
Specific surface areas (m^2/g)	23.71	80.90	65	54.70	22.50	45.10

accompanied by the generation of energy level interleaving, which is beneficial to promoting the separation of holes and electrons, providing more carriers for the gas sensing reaction, thus increasing the gas sensing properties. Fig. 6 shows the gas sensing response of different samples to different concentrations of NH_3 (10–1000 ppm) under UV irradiation at room temperature. It can be concluded from the result that the gas sensing values of all samples are positively correlated with the gas concentration, and the gas sensing response values of TTC-1 samples to NH_3 at any gas concentration are higher than those of other samples. The gas sensing response to 10 ppm NH_3 is 10.4, thus TTC-1 shows a good low detection limit.

According to the comparative study on the gas sensing properties of all samples, it can be seen that TTC-1 is the optimal gas sensing material. As an important index for evaluating the gas sensing material, the gas sensing selectivity of TTC-1 was tested, and the gas sensing responses toward 100 ppm NH_3, methanol, ethanol, toluene, NO_2, CO and formaldehyde were detected, respectively, and the results are displayed in Fig. 7**(a)**. The optimal response value S (%) of the sample towards different gases is as follows: $S_{ammonia}$ (56.9) > $S_{ethanol}$

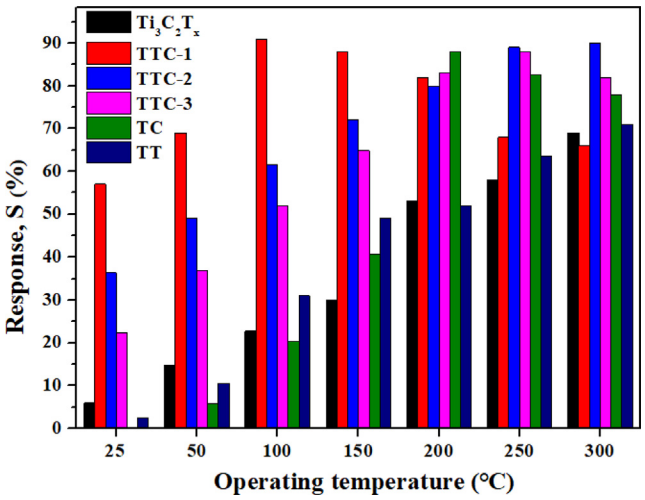

Fig. 5 Gas response of different samples toward 100 ppm NH_3 at different operating temperature under UV irradiation.

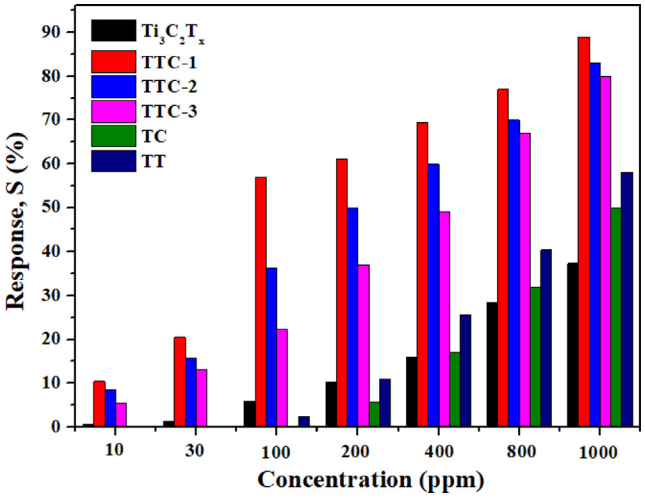

Fig. 6 Gas response of different samples toward different concentration NH_3 at room temperature under UV irradiation.

(36) > S_{CO} (26.9) > $S_{nitrogen\ dioxide}$ (25) > $S_{methanol}$ (19.9) > $S_{formaldehyde}$ (9.96) > $S_{toluene}$ (9.1). The minimum response ratio (α_{min} = $S_{ammonia}/S_{ethanol}$) of TTC-1 sample to NH_3 and other gases with the same concentration reached 1.9, and the maximum response ratio (α_{max} = $S_{ammonia}/S_{toluene}$) is 6.3, indicating that TTC-1 sample has excellent gas sensitivity selectivity. Fig. 7**(b-c)** evaluates the gas sensing stability of TTC-1 sample. The gas sensing response of 100 ppm NH_3 was detected for 10 times within 10 days, and 10 cycles were tested each time. It is found that the gas sensing response of the material fluctuated within the range of ± 2.5 %, and the device shows good cycling stability. It is worth mentioning that resistance of TTC-1 show reducint tendency, putting air back, the resistance increase, indicating that TTC-1 is an n-type semiconductor.

Response time is another important parameter to evaluate the gas sensing materials. The response-recovery time of different samples toward 100 ppm NH3 with UV irradiation at room temperature were measured, the results are shown in Table S1. The response time of TTC-1 toward 100 ppm

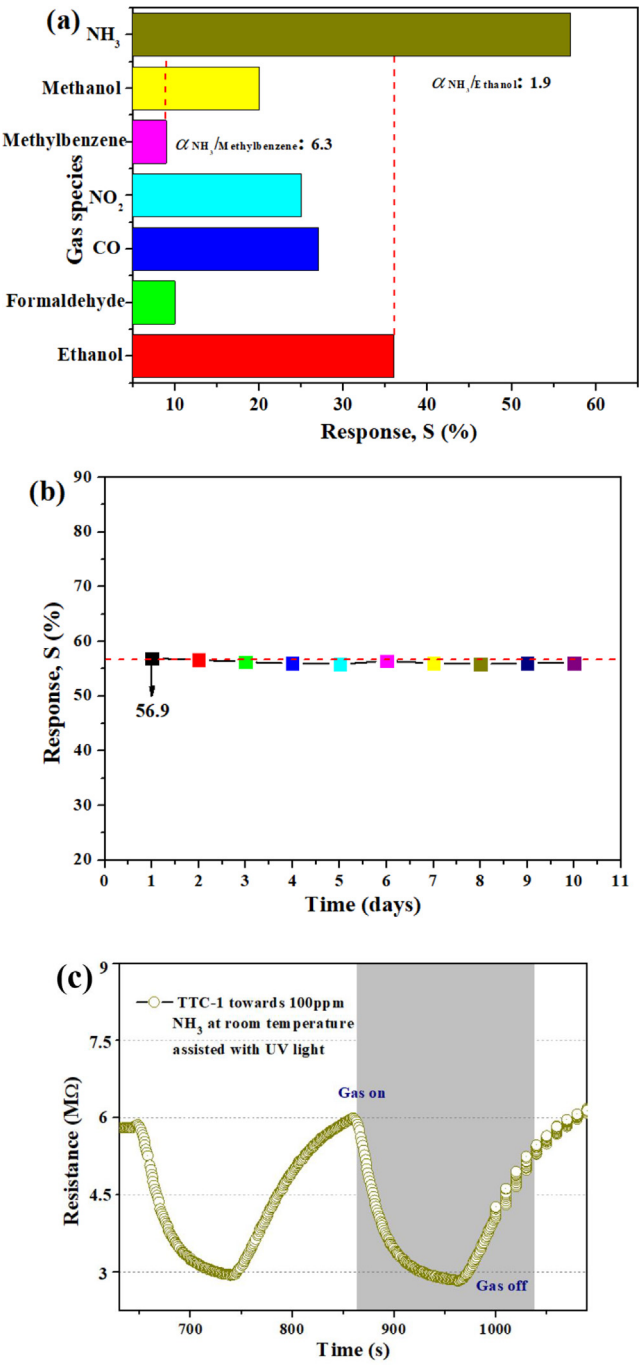

Fig. 7 (a) Gas response of TTC-1 toward 100 ppm different species of gas at room temperature under UV irradiation. (b) The stability of TTC-1 at room temperature to 100 ppm NH_3 under UV irradiation. (c) Dynamic response-recovery curve of TTC-1 towards NH_3 at room temperature assisted with UV light.

NH3 is 75 s and recovery time is 80 s, which exhibites excellent response-recovery properties. TC also shows good response-recovery properties, proving that Ti3C2Tx layer structure plays an important role in carriers transportation.

In order to measure the influence of this work on enhancing the gas sensing performance of MXene materials, the TTC-1 samples obtained in this work were compared with the gas sensing response of 100 ppm NH_3 reported in other literatures.

The results are shown in Table 2. By comparison, the gas sensing response values of TTC-1 samples in this work shows more excellent performacne than those reported in other literatures. It can be concluded that the preparation of MXene composites with TiO_2-CuO heterostructure is an outstanding method to enhance the gas sensitivity of $Ti_3C_2T_x$, and the $Ti_3C_2T_x$-TiO_2-CuO has a good application prospect for the low temperature detection of NH_3.

To further investigate the influence of UV light on the gas sensitivity of TTC-1 materials, the gas sensing properties of TTC-1 samples at room temperature with and without UV light were tested toward different concentrations of NH_3, and the results are shown in Fig. 8. The resistance of TTC-1 toward different target gases with UV irradiation and without UV irradiation at room temperature are shown in **Table S1 and S2**. It can be observed that the gas sensitivities of TTC-1 samples at various gas concentrations (10–1000 ppm) under UV light are higher than those without UV light. The difference can be explained by the activation of UV to TTC-1 sample, which can promote the migration of photogenerated electrons from the VB to CB, making CB provide more free charges to react with adsorb oxygen, resulting in higher gas sensitivity of the material. Therefore, UV light is a necessary factor to enhance the gas sensitivity of TTC-1 sample.

According to analysizing the characterizations of all samples, it can be concluded that TTC-1 sample is an effective gas sensing material for monitoring NH_3 at room temperature coupled with UV exposure. Thus, it is imperative to study the princle of gas sensitivity of TTC-1 sample. Generally, it is wildly accepted that the the gas sensing mechanism of materials can be explained by the resistance change which depends on the chemical reaction on the material surface and the capability of the adsorption and desorption of gas molecules (Wan et al., 2004). Fig. 9**(a)** exhibites the schematic diagram of the principle of gas sensing of TTC-1 without UV exposure. When TTC-1 is deposited in the air, the oxygen molecules are adsorbed on the surface of the material, obtaining electrons, decomposing into oxygen ions and forming an electron depletion layer, which increases the material resistance. When NH_3 is introduced into the surface of TTC-1 material, NH_3 reacts with oxygen anion, and the trapped electrons are released back to the CB of TTC-1 material. During the process, the electron depletion layer of the material get narrower, reducing the material resistance. Compared with the case in the absence of UV irradiation, extra photogenerated electrons will participate in each reaction under UV irradiation (Fig. 9**(b)**), which increases the resistance difference of the material before and after entering the NH_3, thereby improves the gas sensitivity of the material.

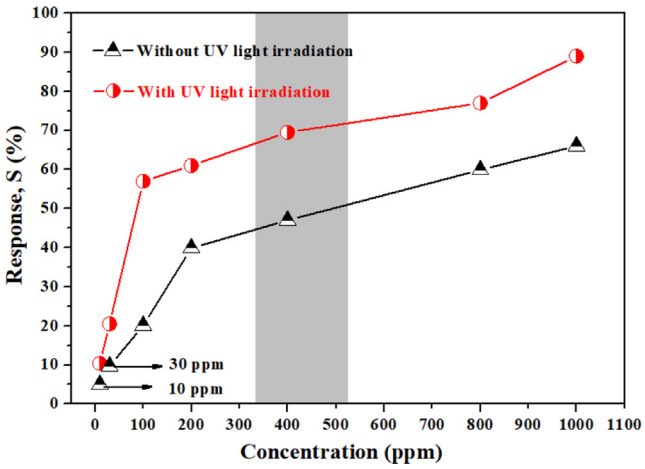

Fig. 8 Gas response of TTC-1 toward different concentrations NH_3 with and without UV light at room temperature.

The construction of TiO_2-CuO heterojunction is also the reason for enhancing the gas sensitivities of materials. The construction of heterojunction effectively reduces the rebinding rate of photogenerated electrons and holes, provides a large number of free charges for the gas sensing reaction, and ensures the effective gas sensitivity reaction. As shown in Fig. 9**(c)**, CuO is a p-type semiconductor, and TiO_2 is a n-type semiconductor. There is a carrier concentration difference at the interface between the two semiconductors. Due to the existence of carrier concentration difference, free electrons and holes migrate and diffuse to the p-zone (CuO) and the n-zone (TiO_2) respectively, so that the electron-hole pairs are effectively separated, thereby enhancing the gas sensitivity of the material. It is worth noting that the TiO_2-CuO heterojunction is attached to the surface of the $Ti_3C_2T_x$ material, which increases the specific surface area of the material and provides a number of active sites for oxygen molecules to adsorb on the material surface. At the same time, TTC-1 sample retains the original layered structure of $Ti_3C_2T_x$ material, which provides a fast channel for electron transport. What' more, for TTC-1 sample, both for reducing gas and oxidizing gas, the increase of specific surface area, the establishment of heterojunction and the retention of MXene sheet structure are beneficial to carrier transport. Therefore, the above structural changes are also beneficial to the gas sensing response of oxidizing gas.

In summary, the combination of UV irradiation, the construction of TiO_2-CuO heterojunction and the preservation of the layered structure of the original $Ti_3C_2T_x$ material led to the TTC-1 sample having higher gas sensing response and

Table 2 The response comparison among this work and other literatures toward NH_3.

Material	Method	Temperature (°C)	Species/Concentration	Response	Ref
GO/WO_3	Hydrothermal	200	NH_3/100 ppm	1.17	47
2D $Ti_3C_2T_x$	Applied directly	Room temperature	NH_3/100 ppm	21%	48
3-D frame $Ti_3C_2T_x$	Self-assembly	Room temperature	NH_3/10 ppm	0.80%	49
Etched $Ti_3C_2T_x$	Alkaline etching	Room temperature	NH_3/100 ppm	28.87%	50
$Ti_3C_2T_x$-TiO_2-CuO	In-situ oxidation	Room temperature coupled with UV irradiation	NH_3/100 ppm	56.90%	This work
PANI-CeO_2	Gaussian process	50	NH3/10 ppm	1.5%	51

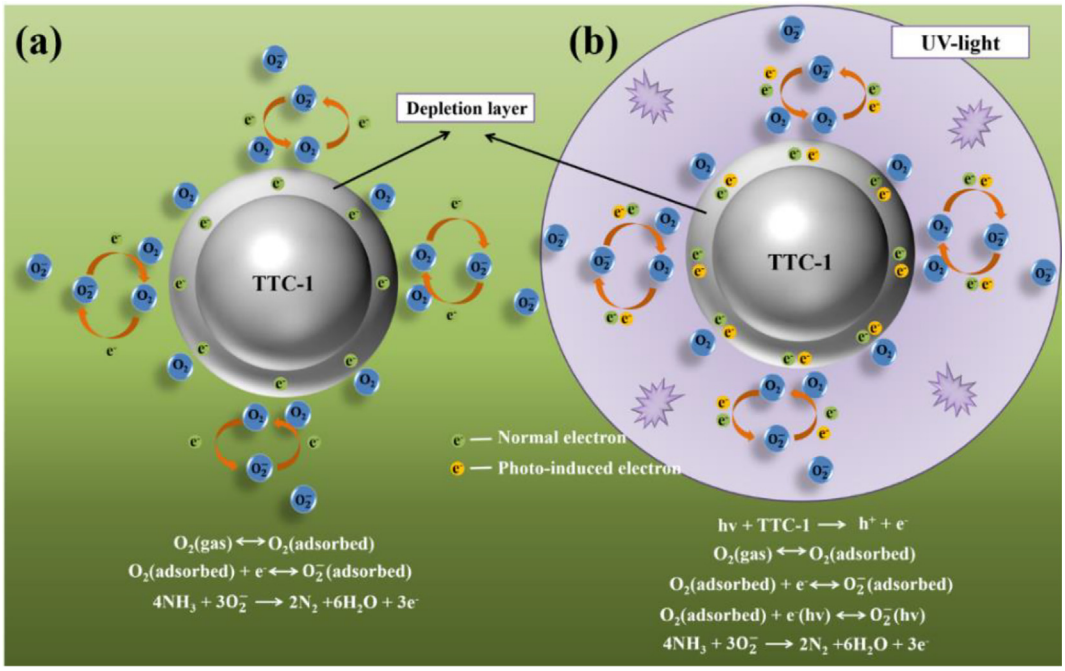

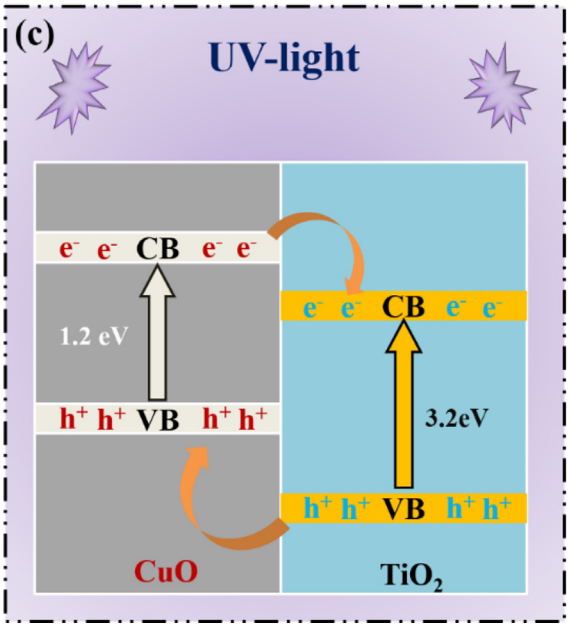

Fig. 9 Schematic diagram of the possible gas sensing mechanism of TTC-1 under UV irradiation.

lower working temperature, making it a gas sensing material with certain advantages.

4. Conclusions

$Ti_3C_2T_x$-TiO_2-CuO composites with different CuO contents were prepared by one-step in-situ oxidation method. TiO_2-CuO composites were also prepared for comparison. By testing the microstructure, phase analysis and gas sensing properties of the samples, the following conclusions are obtained:

(1) TiO_2-CuO heterojunction is attached to the surface of $Ti_3C_2T_x$ material, which enhances the specific surface area and provides a large number of active sites for oxygen adsorption on the material surface. $Ti_3C_2T_x$-TiO_2-CuO composites still maintain the original layered structure of $Ti_3C_2T_x$, which provides a fast channel for electronic transmission.

(2) The $Ti_3C_2T_x$-TiO_2-CuO composite exhibits n-type semiconductor properties. The composite with 0.01% CuO exhibits the best gas sensing response, and the response value towards 100 ppm NH_3 at room temperature can reach 56.9%, which is 89.8% higher than that of pure $Ti_3C_2T_x$. At the optimal working tem-

perature (100° C), the response value to 100 ppm NH_3 can reach 91.1 %, and the material has excellent gas sensing selectivity and stability.

(3) The improvement of the gas sensitivity of the material is attributed to the excitation of the photogenerated electrons and holes of the material by the irradiation of UV light, which provides more free charges for the gas sensitivity reaction and makes the resistance difference of the material larger before and after the target gas is introduced. The construction of TiO_2-CuO heterojunction effectively reduces the electron-hole recombination rate, provides a large number of electrons for the gas-sensitive reaction, and ensures the effective conduct of gas-sensitive reaction. The TiO_2-CuO heterojunction is attached to the surface of $Ti_3C_2T_x$ material, which increases the specific surface area of the material and provides more active sites for oxygen molecules to adsorb on the surface of the material. At the same time, TTC-1 sample retains the original layered structure of $Ti_3C_2T_x$ material, which provides a fast channel for electron transport.

Acknowledgement

This research was funded by National Natural Science Foundation of China, No. 51864028, NSAF No. U2030207; Yunnan Fundamental Research Projects, No. 202201BE070001-018; Yunnan Province Funds for Distinguished Young Scientists, No. 2019FJ005; Science Research Foundation of Yunnan Provincial Education Department, No. 2022J0441.

Appendix A. Supplementary data

Supplementary data to this article can be found online at https://doi.org/10.1016/j.arabjc.2023.104808.

References

Akhtar, N., Rani, M., Mahmood, A., Saba, H., Khan, S., Murtaza, G., Hegazy, H., Alobaid, A., 2021. Synthesis and characterization of MXene/$BiCr_2O_4$ nanocomposite with excellent electrochemical properties. J Mater Res Technol. 15, 2007–2015. https://doi.org/10.1016/j.jmrt.2021.08.101.

Alev, O., Sennik, E., 2018. Improved gas sensing performance of p-copper oxide thin film/n-TiO_2 nanotubes heterostructure. J. Alloys Comp. 749, 221–228. https://doi.org/10.1016/j.jallcom.2018.03.268.

Aliha, H.M., Khodadadi, A.A., Mortazavi, Y., 2013. The sensing behaviour of metal oxides (ZnO, CuO and Sm_2O_3) doped-SnO_2 for detection of low concentrations of chlorinated volatile organic compounds. Sens. Actuators, B. B181, 637–643. https://doi.org/10.1016/j.snb.2013.02.055.

Alothman, Z.A., Wabaidur, S.M., 2019. Application of carbon nanotubes in extraction and chromatographic analysis: A review. Arab. J. Chem. 12, 633–651. https://doi.org/10.1016/j.arabjc.2018.05.012.

Amparo, L.R., Bernadine, M.F., Elliot, P.G., 2008. A novel approach for calculating starch crystallinity and its correlation with double helix content: A combined XRD and NMR study. Biopolymers 89, 761–768. https://doi.org/10.1002/bip.21005.

Chan, C.K., Yao, X., 2008. Air pollution in mega cities in China. Atmos Environ. 42, 1–42. https://doi.org/10.1016/j.atmosenv.2007.09.003.

Chen, H., Liu, Y., Xie, C., Wu, J., Zeng, D., 2012. A comparative study on UV light activated porous TiO_2 and ZnO film sensors for gas sensing at room temperature. Ceram. Int. 38, 503–509. https://doi.org/10.1016/j.ceramint.2011.07.035.

Chen, Y., Xie, X., Xin, X., Tang, Z., Xu, Y., 2019. $Ti_3C_2T_x$-Based Three-Dimensional Hydrogel by a Graphene Oxide-Assisted Self-Convergence Process for Enhanced Photoredox Catalysis. ACS Nano 13, 295–304. https://doi.org/10.1021/acsnano.8b06136.

Ciżmana, A., 2020. Effect of the iron content on the structure and electrical properties of sodium borosilicate glasses: XRD, TEM, Mössbauer, FTIR and DIS spectroscopy study. J Non-Cryst. Solids. 531,. https://doi.org/10.1016/j.jnoncrysol.2019.119847 119847.

Cui, J., Shi, L., Xie, T., Wang, D., Lin, Y., 2016. UV-light illumination room temperature HCHO gas-sensing mechanism of ZnO with different nanostructures. Sens. Actuators, B. 227, 220–226. https://doi.org/10.1016/j.snb.2015.12.010.

Deng, Y., Shen, Y., Du, Y., Goto, T., Zhang, J.F., 2022. A novel electrode hybrid of N-$Ti_3C_2T_x$/C/CuS fabricated using ZIF-67 as an intermediate derivation for superhigh electrochemical properties of supercapacitors. J Mater Res Technol. 19, 3507–3520. https://doi.org/10.1016/j.jmrt.2022.06.118.

Gasso, S., Sohal, M.K., Mahajan, A., 2022. MXene modulated SnO_2 gas sensor for ultra-responsive room-temperature detection of NO_2. Sens. Actuators, B. 357,. https://doi.org/10.1016/j.snb.2022.131427 131427.

Hang, N., Zhang, S., Yang, W., 2017. Efficient exfoliation of g-C_3N_4 and NO_2 sensing behavior of graphene/g-C_3N_4 nanocomposite. Sens. Actuators, B. 248, 940–948. https://doi.org/10.1016/j.snb.2017.01.199.

Hou, M., Gao, J.Y., Yang, L., Guo, S.H., Hu, T., Li, Y.X., 2021. Room temperature gas sensing under UV light irradiation for $Ti_3C_2T_x$ MXene derived lamellar TiO_2-C/g-C_3N_4 composites. Appl. Surf. Sci. 535,. https://doi.org/10.1016/j.apsusc.2020.147666 147666.

Hou, M., Guo, S.H., Yang, L., Gao, J.Y., Hu, T., Wang, X.W., 2021. Improvement of Gas Sensing Property for Two-Dimensional $Ti_3C_2T_x$ treated with Oxygen Plasma by Microwave Energy Excitation. Ceram. Int. 47, 7728–7737. https://doi.org/10.1016/j.ceramint.2020.11.117.

Kanaparthi, S., Singh, S.G., 2020. Highly sensitive and ultra-fast responsive ammonia gas sensor based on 2D ZnO nanoflakes. Materials Sci. Energy Tech. 3, 91–96. https://doi.org/10.1016/j.mset.2019.10.010.

Karaduman, I., Yıldız, D., Sincar, M., Acar, S., 2014. UV light activated gas sensor for NO_2 detection. Mater. Sci. Semicond. Process. 28, 43–47. https://doi.org/10.1016/j.mssp.2014.04.011.

Khudher, H.H., Abd, J.A., 2021. Variation Resistance of different operation temperature of NO_2 and NH_3 gases for the Ag-doped SiC gas sensor. J. Phys: Conference Series. 1973,. https://doi.org/10.1088/1742-6596/1973/1/012140 012140.

Kim, S.J., Koh, H.J., Ren, C.E., Kwon, O., Maleski, K., Cho, S.Y., Anasori, B., Kim, C.K., Choi, Y.K., Kim, J., Gogotsi, Y., Jung, H. T., 2018. Metallic $Ti_3C_2T_x$ MXene Gas Sensors with Ultrahigh Signal-to-Noise Ratio. ACS Nano 12, 986–993.

Kou, X., Wang, C., Ding, M., 2016. Synthesis of Co-doped SnO_2 nanofibers and their enhanced gas-sensing properties. Sens. Actuators, B. 236, 425–432. https://doi.org/10.1016/j.snb.2016.06.006.

Lai, Y., Huang, J., Zhang, H., Subramaniam, V., 2010. Nitrogen-doped TiO_2 nanotube array films with enhanced photocatalytic activity under various light sources. J. Hazard. Mater. 184, 855–863. https://doi.org/10.1016/j.jhazmat.2010.08.121.

Late, D.J., Doneus, T., Bougouma, M., 2014. Single-layer $MoSe_2$ based NH_3 gas sensor. Appl. Phys. Lett. 105,. https://doi.org/10.1063/1.4903358 233103.

Lei, J.C., Zhang, Q., Zhao, Z.Y., Chen, Y.Z., Gao, J., Tong, J.H., Peng, F., Xiao, H., 2020. One-Step Fabrication of Nanocrystalline Nanonetwork SnO_2 Gas Sensors by Integrated Multilaser Processing. Adv. Mater Technol-US. 5, 2000281. https://doi.org/10.1002/admt.202000281.

Li, Q., Li, Y., Zeng, W., 2021. Preparation and Application of 2D MXene-Based Gas Sensors: A Review. Chemosensors. 9, 225. https://doi.org/10.3390/chemosensors9080225.

Li, J., Zhao, C.H., Wang, Y.J., Zhang, R.J., Zou, C., Zhou, Y., 2022. Mesoporous WS2-Decorated Cellulose Nanofiber-Templated CuO Heterostructures for High-Performance Chemiresistive Hydrogen Sulfide Sensors. Anal. Chem. 94 (46), 16160–16170.

Meng, F.L., Hou, N.N., Ge, S., Sun, B., Jin, Z., Shen, W., Kong, L.T., Guo, Z., Sun, Y.F., 2015. Flower-like hierarchical structures consisting of porous single-crystalline ZnO nanosheets and their gas sensing properties to volatile organic compounds (VOCs). J. Alloys Comp. 626, 124–130. https://doi.org/10.1016/j.jallcom.2014.11.175.

Miller, D., Akbar, S., Morris, P., 2014. Nanoscale metal oxide-based heterojunctions for gas sensing: a review. Sens. Actuators, B. 204, 250–272. https://doi.org/10.1016/j.snb.2014.07.074.

Qin, Y., Gui, H.Y., Bai, Y., Liu, S.C., 2022. Enhanced NH_3 sensing performance at ppb level derived from $Ti_3C_2T_x$-supported ZnTi-LDHs nanocomposite with similar metal-semiconductor heterostructure. Sens. Actuators, B. 352,. https://doi.org/10.1016/j.snb.2021.131077 131077.

Shahabuddin, M., Sharma, A., Kumar, J., Tomar, M., Umar, A., 2014. Metal clusters activated SnO_2 thin film for low level detection of NH_3 gas. Sens. Actuators, B. 194, 410–418. https://doi.org/10.1016/j.snb.2013.12.097.

Shkir, M., Ben Gouider Trabelsi, A., Alkallas, F.H., Alfaify, S., 2022. High performance of the rare earth (Er, Gd & Pr) doped MoO3 thin films for advanced applications towards ammonia gas sensing. J Mater Res Technol. 20, 4556–4565. https://doi.org/10.1016/j.jmrt.2022.08.144.

Sun, S.B., Wang, M.W., Chang, X.T., Jiang, Y.C., Zhang, D.Z., 2020. $W_{18}O_{49}$/$Ti_3C_2T_x$ Mxene nanocomposites for highly sensitive acetone gas sensor with low detection limit. Sens. Actuators, B. 304,. https://doi.org/10.1016/j.snb.2019.127274 127274.

Wan, Q., Li, Q.H., Chen, Y.J., Wang, T.H., He, X.L., Li, J.P., Lin, C. L., 2004. Fabrication and ethanol sensing characteristics of Zn nanowire gas sensors. Appl. Phys. Lett. 84, 3654–3656. https://doi.org/10.1063/1.1738932.

Wang, X.C., Chen, X.F., Thomas, A., Fu, X.Z., Antonietti, M., 2009. Metal-containing carbon nitride compounds: a new functional organic–metal hybrid material. Adv. Mater. 21, 1609–1612. https://doi.org/10.1002/adma.200802627.

Wang, G., Wang, H., Ling, Y., Tang, Y., Yang, X., Fitzmorris, R.C., Wang, C., Zhang, J.Z., Li, Y., 2011. Hydrogen-Treated TiO2 Nanowire Arrays for Photoelectrochemical Water Splitting. Nano. Lett. 11, 3026–3033. https://doi.org/10.1021/nl201766h.

Wang, Y.J., Zhou, Y., Wang, Y.H., Zhang, R.J., Li, J., Li, X., Zang, Z.G., 2021. Conductometric room temperature ammonia sensors based on titanium dioxide nanoparticles decorated thin black phosphorus nanosheets. Sens. Actuators B 349,. https://doi.org/10.1016/j.snb.2021.130770 130770.

Wu, D.Z., Peng, Q., Wu, S., Wang, G.S., Deng, L., Tai, H.L., Wang, L.Y., 2018. A Simple Graphene NH_3 Gas Sensor via Laser Direct Writing. Sensors (Basel). 18, 4405. https://doi.org/10.3390/s18124405.

Xie, X., Zhang, N., Tang, Z., Anpo, M., Xu, Y., 2018. $Ti_3C_2T_x$ MXene as a Janus cocatalyst for concurrent promoted photoactivity and inhibited photocorrosion. Appl. Catal. B. 237, 43–49. https://doi.org/10.1016/j.apcatb.2018.05.070.

Xu, H.P., Liu, C.H., Chen, M.H., Wang, Q., Li, L.B., Dai, Y., 2022. Hydrothermal synthesis of one-dimensional α-MoO_3 nanomaterials and its unique sensing mechanism for ethanol. Arab. J. Chem. 15,. https://doi.org/10.1016/j.arabjc.2022.104083 104083.

Xu, S., Wei, G., Li, J., Ji, Y., Klyui, N., Lzotov, V., Han, W., 2017. Binder-free $Ti_3C_2T_x$ MXene electrode film for supercapacitor produced by electrophoretic deposition method. Chem. Eng. J. 317, 1026–1036. https://doi.org/10.1016/j.cej.2017.02.144.

Yuan, W., Yang, K., Peng, H., Li, F., Yin, F., 2018. A flexible VOCs sensor based on a 3D MXene framework with a high sensing performance. J. Mater. Chem. A. 6, 18116–18124. https://doi.org/10.1039/C8TA06928J.

Zhang, Y.J., Jiang, Y.D., Duan, Z.H., Wu, Y.W., Huang, Q., Yuan, Z., Li, X., Tai, H.L., 2022. Edge-enriched MoS_2 nanosheets modified porous nanosheet-assembled hierarchical In_2O_3 microflowers for room temperature detection of NO_2 with ultra-high sensitivity and selectivity. J. Hazrad. Mater. 15,. https://doi.org/10.1016/j.jhazmat.2022.128836 128836.

Zhang, S., Lei, T., Li, D., Zhang, G., Xie, C., 2014. UV light activation of TiO_2 for sensing formaldehyde: How to be sensitive, recovering fast, and humidity less sensitive. Sens. Actuators, B. 202, 964–970. https://doi.org/10.1016/j.snb.2014.06.063.

Zhao, Q., Sun, D.M., Wang, S., Duan, Z.H., Yuan, Z., Wei, G.F., Xiu, J.L., Tai, H.L., Jiang, Y.D., 2021. Enhanced Blocking Effect: A New Strategy to Improve the NO_2 Sensing Performance of $Ti_3C_2T_x$ by γ-Poly(l-glutamic acid) Modification. ACS Sens. 6, 2858–2867 https://10.1021/acssensors.1c00132.

Zhao, Q.N., Zhang, Y.J., Duan, Z.H., Wang, S., Lu, C., Jiang, Y.D., Tai, H.L., 2020. A review on $Ti_3C_2T_x$-based nanomaterials: synthesis and applications in gas and humidity sensors. Rare Met. 40 (6), 1459–1476 https://link.springer.com/article/10.1007/s12598-020-01602-2.

Zhou, Y., Wang, Y. H., Wang, Y. J., Yu, H. C., Zhang, R. J., Li, J., Zang, Z. G., Li, X. 2021. MXene $Ti_3C_2T_x$-Derived Nitrogen-Functionalized Heterophase TiO_2 Homojunctions for Room-Temperature Trace Ammonia Gas Sensing. ACS Appl. Mater. Interfaces. 13, 47:5 6485-56497. https://doi.org/10.1021/acsami.1c17429.